A Common Ground Switched-Quasi-*Z*-Source Bidirectional DC-DC Converter with Wide-Voltage-Gain Range for EVs with Hybrid Energy Sources

Yun Zhang, *Member, IEEE*, Qiangqiang Liu, Jing Li, *Member, IEEE*, and Mark Sumner, *Senior Member, IEEE*

Abstract—A common ground switched-quasi-Z-source bidirectional DC-DC converter is proposed for electric vehicles (EVs) with hybrid energy sources. The proposed converter is based on the traditional two-level quasi-Z-source bidirectional DC-DC converter, changing the position of the main power switch. It has the advantages of a wide voltage gain range, a lower voltage stress across the power switches, and an absolute common ground. The operating principle, the voltage and current stresses on the power switches, the comparisons with the other converters, the small signal analysis and the controller design are presented in this paper. Finally, a 300W prototype with U_{high}=240V and U_{low}=40~120V is developed, and the experimental results validate the performance and the feasibility of the proposed converter.

Index Terms—Bidirectional DC-DC converter, common ground, EVs, hybrid energy sources, switched-quasi-Z-source, wide voltage gain range.

I. INTRODUCTION

With the increase of per capita car ownership in the world, the increases in fossil fuel consumption and greenhouse gas emission are having a serious effect on the climate and environment [1]-[5]. New energy vehicles with renewable energy as the power source, which can achieve operation with zero pollution emissions, are considered as one of the solutions to effectively alleviate the energy crisis and the environmental pollution associated with transportation [6], [7]. As one of the most important "new energy" vehicles, electric vehicles with hybrid energy sources mainly comprise high energy density power batteries and high power density super capacitors. The low-voltage batteries are used to maintain the high voltage of the DC bus during steady-state, even when the required energy has low-frequency fluctuations. The super capacitors can be used to provide or absorb high-frequency instantaneous power during the electric vehicle's accelerating or braking process. Thus, these two hybrid energy sources can greatly reduce the

Y. Zhang, Q. Liu are with the School of Electrical and Information Engineering, Tianjin University, Nankai, Tianjin, China (e-mail: zhangy@tju.edu.cn; lqqcumt@163.com).

J. Li is with the Department of Electrical and Electronic Engineering, University of Nottingham Ningbo China, Ningbo, China (e-mail: Jing.Li@nottingham.edu.cn).

M. Sumner is with the Department of Electrical and Electronic Engineering, University of Nottingham, Nottingham, England, U.K (e-mail: mark.sumner@nottingham.ac.uk).

degradation impact on the power batteries caused by the sudden load change of the electric vehicle, and also improve the dynamic response of the whole powertrain system [8], [9].

The voltage level of hybrid energy sources for electric vehicles is relatively low. In order to realize the matching of the voltage levels between the hybrid energy sources and the high voltage DC bus, as well as the bidirectional power flow of energy sources, a wide voltage-gain range bidirectional DC-DC converter is needed to interface the energy sources and the DC bus.

With regard to the wide voltage-gain range bidirectional DC-DC converter, basically, it can be classified into two categories: isolated and non-isolated. The isolated types of bidirectional converters include Fly-back converters, forward converters, half-bridge and full-bridge bidirectional converters. One of the advantages of these bidirectional DC-DC converters is that they have a wide voltage-gain range in the step-up and step-down modes. Although the Fly-back converter has a simple structure and can be controlled easily, the leakage inductor loss caused by the high frequency transformer mean the converter has a low efficiency. In addition, the leakage inductor causes high voltage spikes, which means the power switches see a high voltage stress.

Non-isolated bidirectional converters include conventional two-level converters and multilevel converters, Cuk/Sepic/Zeta converters, coupled-inductor converters, switched-capacitor and switched-inductor converters, Z-source and quasi-Z-source converters. The conventional two-level converters have a high voltage stress on the power switches, a narrow voltage-gain range, and their efficiencies and dynamic responses are limited by the extreme duty cycles of the power switches. Therefore, they are not suitable for the hybrid energy sources system of electric vehicles. As to the three-level DC-DC converters, although the voltage stress on the power switches is significantly reduced, the practical voltage gain in the step-up and step-down modes is relatively low due to the parasitic parameters [10], [11]. Multi-level DC-DC converters have a wide voltage gain range, but they need more power switches, other additional hardware circuits and a control strategy to maintain the balance of the voltage stress on the power switches [12]. Although the voltage gain range of the Cuk/Sepic/Zeta converters is wider, the cascaded structures limit the conversion efficiency [13]-[15]. Coupled-inductor DC-DC converters can achieve a high voltage gain by adjusting the turns ratio of the coupled inductor, but they require more power switches and need to address the problem of the leakage inductance, which make their structure more complex. In addition, the power conversion and transmission capability of the converter is also limited by the performance of the coupled inductor [16]-[18].

The structures and control schemes of the Z-source, the quasi-Z-source and the switched-capacitor DC-DC converters are simple and easy to expand, and the capacitors in these converters deliver energy through different paths during the charge and the discharge processes. Thus, a high voltage gain can be achieved [19]-[22]. Switched-inductor bidirectional DC-DC converters can also achieve a wide voltage gain range and a low voltage stress while avoiding extreme duty cycles. However, more inductors limit the power density [23], [24].

A new non-isolated single capacitor bidirectional DC-DC converter is presented in [25]. Although it has a wide voltage gain range, the voltage stress on the power switches is relatively high. In [22], a switched-capacitor-based DC-DC converter is proposed. Although the voltage gain is improved, more devices are used, and the converter does not have a common ground. A bidirectional switched-capacitor DC-DC converter is presented in [26]. This converter improves the efficiency, but the converter needs more power switches. A hybrid bidirectional converter with a switched-capacitor cell, which is suitable for a DC microgrid, is proposed in [27]. It has a wider voltage gain range and lower power voltage stress across the power switches, but the converter does not have an absolute common ground between the input and output sides, which produces an additional du/dt issue between the input and output grounds. Thus, its applications are limited. In [28], a novel coupled-inductor bidirectional DC-DC converter is proposed with increased voltage gain. However, the leakage inductance of the coupled inductor and the additional du/dt problems between the input and output grounds should be considered additionally, and the voltage stress on the power switches that are near the high voltage side is too high.

This paper presents a novel switched-quasi-Z-source bidirectional DC-DC converter for EVs with hybrid energy sources, which not only achieves a wide voltage gain range, but also has a common ground. The proposed converter is based on the traditional two-level quasi-Z-source bidirectional DC-DC converter: it simply changes the position of the main power switch. As well as a wide voltage gain range and a low voltage stress on power switches, this converter also has a simple structure. As a result, the proposed converter can select the power switches with the low rated voltage, and the low on-state resistance, which in turn can improve the conversion efficiency. Simultaneously, the voltage-gain of the proposed converter is just reduced a bit, which can still meet the requirement of the application of EVs with hybrid energy sources. The absolutely common ground also avoids the additional du/dt issue between the input and output grounds, which is beneficial for the operation of the proposed converter.

The structure of the paper is organized as follows. Section II introduces the configuration of the proposed converter and analyzes the operating principle in detail. The design and analysis of the converter are given in Section III. The experimental results and analysis are shown in Section IV. Finally, Section V presents conclusions.

II. OPERATING PRINCIPLE AND ANALYSIS OF THE PROPOSED CONVERTER

A. Configuration of the Proposed Converter

The configuration of the proposed bidirectional DC-DC converter is shown in Fig.1. It can be seen that the proposed converter consists of a switched-quasi-Z-source network (L_1, L_2, C_1, C_2 and Q_2), power switches Q_1 and Q_3, and high/low voltage side energy storage/filter capacitors C_{high} and C_{low}. The gate signals S_2 and S_3 of the power switches Q_2 and Q_3 are identical, and they are complementary to the gate signal S_1 of Q_1. The proposed converter can operate either in the step-up or in the step-down mode, enabling the bidirectional power flow between the high-voltage and low-voltage sides.
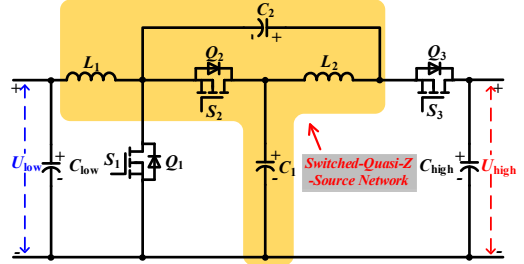

Fig.1 Configuration of the proposed converter.

B. Operating Principle of the Proposed Converter

To simplify the analysis, the following assumptions are made.

1) All the components are ideal, ignoring the ON-STATE resistance R_{DS}(on) of the power switches and equivalent series resistance(ESR) of the inductors and capacitors.

2) The currents of the inductors and voltages of the capacitors increase and decrease linearly.

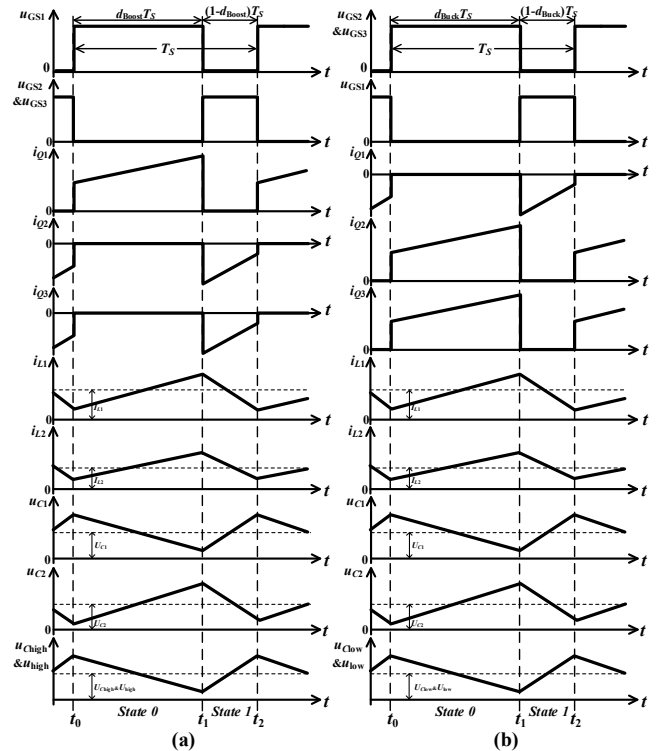3) The voltages across capacitors are constant.

Fig.2 Typical waveforms of the proposed converter. (a) Step-up mode. (b) Step-down mode.

The two main operating modes of the proposed converter are given as follows:

Mode I. *Step-Up Mode of the Proposed Converter*

When the proposed converter operates in the step-up mode, namely the energy flows from the low voltage side to the high voltage side. In this operating mode, Q_1 operates as a main power switch, and Q_2 and Q_3 are the synchronous rectifiers. The duty cycles of the gate signals S_1, S_2 and S_3 are taken as $d_1=1-d_2=1-d_3=d_{Boost}$. The typical waveforms of the proposed converter in continuous conduction mode (CCM) are shown in Fig.2 (a), and the corresponding current flow paths in one switching period are illustrated in Fig.3 (a) and (b).

State 0 [t_0-t_1]: When $S_1S_2S_3$=100, Q_1 is turned on, and Q_2 and Q_3 are turned off, the current flow paths are shown in Fig.3 (a). During this state, the inductor L_1 is charged by U_{low} through Q_1, while the capacitor C_1 is discharged, and the energy is transferred to the capacitor C_2 and the inductor L_2 through Q_1. Capacitor C_{high} is also discharged to supply the energy for the load R_{load_Boost}. According to Fig.3 (a), the following equations can be derived in state 0:

$$\begin{cases} U_{L1} = U_{low} \\ U_{L2} = U_{C1} - U_{C2} \\ U_{high} = U_{Chigh} \end{cases} \quad (1)$$

$$\begin{cases} i_{C1\_d_{Boost}} = -i_{L2} \\ i_{C2\_d_{Boost}} = i_{L2} \\ i_{Chigh\_d_{Boost}} = -I_{high} \end{cases} \quad (2)$$

State 1 [t_1-t_2]: When $S_1S_2S_3$=011, Q_1 is turned off, and Q_2 and Q_3 are reversely turned on. The current flow paths are shown in Fig.3 (b). During this interval, the input voltage U_{low} and the inductor L_1 charge the capacitor C_1 in series. The capacitor C_2 is connected in parallel with inductor L_2, then connected with U_{low} and L_1 in series to charge the capacitor C_{high} and provide the energy for the load. As a result, the output voltage U_{high} is boosted up, and is much higher than the input voltage U_{low}. According to Fig.3 (b), the following equations can also be obtained in state 1:

$$\begin{cases} U_{L1} = U_{low} - U_{C1} \\ U_{L2} = U_{C1} - U_{Chigh} \\ U_{Chigh} = U_{C2} + U_{C1} \\ U_{high} = U_{Chigh} \end{cases} \quad (3)$$

$$\begin{cases} i_{C1\_(1-d_{Boost})} = i_{L1} + i_{C2\_(1-d_{Boost})} - i_{L2} \\ i_{Chigh\_(1-d_{Boost})} = i_{L2} - i_{C2\_(1-d_{Boost})} - I_{high} \end{cases} \quad (4)$$

By applying the volt-second balance principle on inductors L_1 and L_2 with (1) and (3), the relationship between the voltage gain M_{Boost} and the duty cycle d_{Boost} in CCM can be obtained as

$$M_{Boost} = \frac{1+d_{Boost}}{1-d_{Boost}} \quad (5)$$

and the voltage stresses across the capacitors C_1 and C_2 can be expressed as

$$\begin{cases} U_{C1} = \frac{U_{low}}{1-d_{Boost}} = \frac{U_{high}}{1+d_{Boost}} \\ U_{C2} = \frac{d_{Boost}U_{low}}{1-d_{Boost}} = \frac{d_{Boost}U_{high}}{1+d_{Boost}} \end{cases} \quad (6)$$

By applying the ampere-second balance principle on capacitors with (2) and (4), the average inductor currents I_{L1} and I_{L2} can be obtained as

$$\begin{cases} I_{L1} = \frac{1+d_{Boost}}{1-d_{Boost}} I_{high} \\ I_{L2} = I_{high} \end{cases} \quad (7)$$

Mode II. Step-Down Mode of the Proposed Converter

When the proposed converter operates in the step-down mode, namely the energy flows from the high voltage side to the low voltage side. In this operating mode, Q_2 and Q_3 operate as the main power switches, and Q_1 is the synchronous rectifier. The duty cycles of the gate signals S_2, S_3 and S_1 are taken as $d_2=d_3=1-d_1=d_{Buck}$. The typical waveforms of the proposed converter in CCM are shown in Fig.2 (b), and the corresponding current flow paths in one switching period are illustrated in Fig.4 (a) and (b).

State 0 [t_0-t_1]: When $S_1S_2S_3$=011, Q_1 is turned off, and Q_2 and Q_3 are turned on, the current flow paths are shown in Fig.4 (a). During this state, L_1, L_2, C_2, and the low voltage side load R_{load_Buck} are charged by U_{high} through Q_3 and Q_2, while C_1 is discharged for L_1 and R_{load_Buck} through Q_2. Then, the following equations can be derived in state 0:

$$\begin{cases} U_{L2} = U_{high} - U_{C1} \\ U_{L1} = U_{C1} - U_{low} \\ U_{C1} + U_{C2} = U_{high} \\ U_{high} = U_{C3} \end{cases} \quad (8)$$

$$\begin{cases} i_{C1\_d_{Buck}} = i_{C2\_d_{Buck}} - i_{L1} + i_{L2} \\ i_{C2\_d_{Buck}} = I_{high} - i_{C3\_d_{Buck}} - i_{L2} \\ i_{L1} = I_{low} + i_{Clow\_d_{Buck}} \end{cases} \quad (9)$$

State 1 [t_1-t_2]: When $S_1S_2S_3$=100, Q_1 is reversely turned on, Q_2 and Q_3 are turned off. The current flow paths are shown in Fig.4 (b). During this state, U_{high} charges C_{high}, while C_2 is connected in series with L_2 to charge C_1 through Q_1. L_1 also supplies energy for the load R_{load_Buck} through Q_1. By means of Fig.4 (b), the following equations can be obtained in state 1:

$$\begin{cases} U_{L1} = U_{C2} - U_{C1} \\ U_{L2} = -U_{low} \\ U_{high} = U_{C3} \end{cases} \quad (10)$$

$$\begin{cases} i_{C1\_(1-d_{Buck})} = i_{L2} \\ i_{C2\_(1-d_{Buck})} = -i_{L2} \\ i_{C3\_(1-d_{Buck})} = I_{high} \\ i_{L1} = I_{low} + i_{Clow\_(1-d_{Buck})} \end{cases} \quad (11)$$

By applying the volt-second balance principle on L_1 and L_2 with (8) and (10), the relationship between the voltage gain M_{Buck} and the duty cycle d_{Buck} in CCM can be obtained as

$$M_{Buck} = \frac{d_{Buck}}{2-d_{Buck}} \quad (12)$$

and the voltage stresses across the capacitors C_1 and C_2 can be described as

$$\begin{cases} U_{C1} = \dfrac{U_{\text{low}}}{d_{\text{Buck}}} = \dfrac{U_{\text{high}}}{2 - d_{\text{Buck}}} \\ U_{C2} = \dfrac{(1 - d_{\text{Buck}})U_{\text{low}}}{d_{\text{Buck}}} = \dfrac{(1 - d_{\text{Buck}})U_{\text{high}}}{2 - d_{\text{Buck}}} \end{cases} \quad (13)$$

By applying the ampere-second balance principle on capacitors with (9) and (11), the average inductor currents I_{L1} and I_{L2} in the step-down mode can be written as

$$\begin{cases} I_{L1} = I_{\text{low}} \\ I_{L2} = \dfrac{d_{\text{Buck}}}{2 - d_{\text{Buck}}} I_{\text{low}} \end{cases} \quad (14)$$
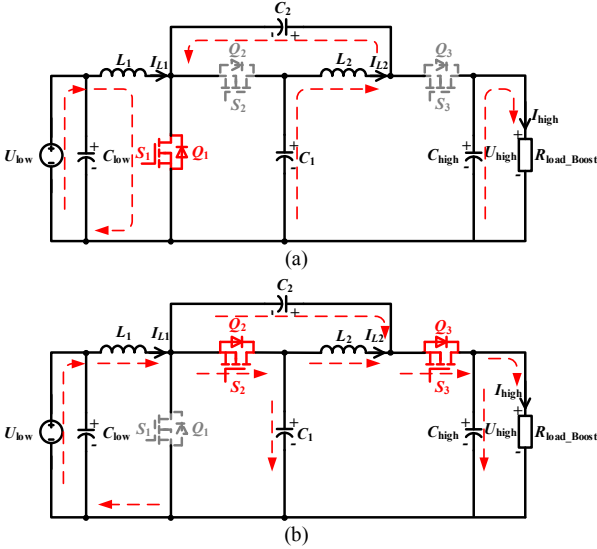

(a)

(b)

Fig.3 Current-flow paths of the proposed converter in the step-up mode. (a) State 0: $S_1 S_2 S_3 = 100$. (b) State 1: $S_1 S_2 S_3 = 011$.
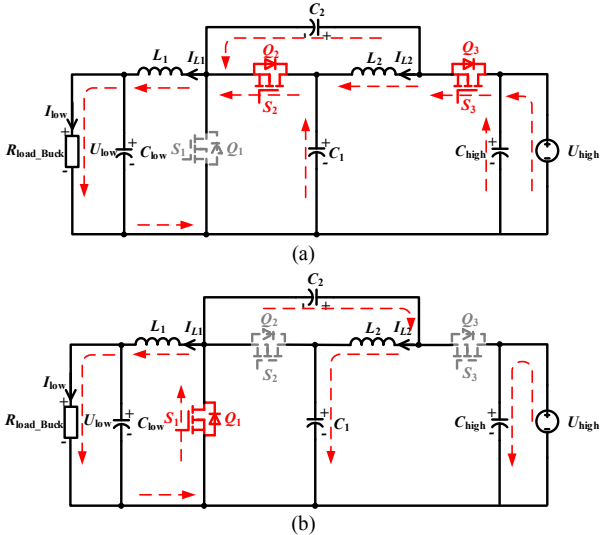

(a)

(b)

Fig.4 Current-flow paths of the proposed converter in the step-down mode. (a) State 0: $S_1 S_2 S_3 = 011$. (b) State 1: $S_1 S_2 S_3 = 100$.

C. Bidirectional Operating Control Strategy of the Proposed Converter

The bidirectional power flow control strategy of the proposed switched-quasi-Z-source converter is shown in Fig.5. The proposed converter is interfaced between the high voltage DC bus and the low voltage super capacitor bank.

The two operating modes of the converter in the hybrid energy sources system can be switched by judging the positive or negative polar of the control signal I_{sgn}, which should be provided by the energy management system omitted in this paper.
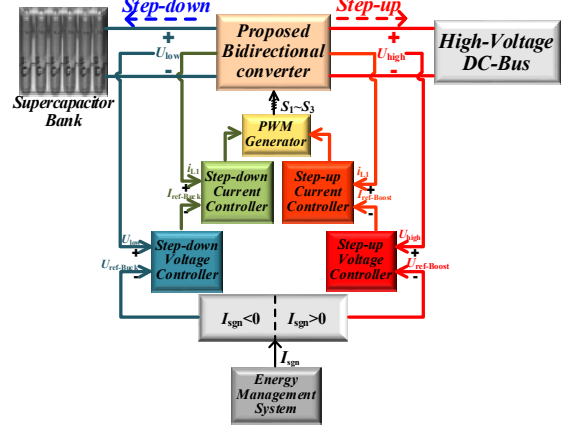

Fig.5 Bidirectional power flow control strategy of the proposed converter.

1). When $I_{\text{sgn}} > 0$, the controller enables the converter to operate in the step-up mode. At this point, the step-up mode reference voltage $U_{\text{ref-Boost}}$ is output by the step-up mode voltage controller with consideration of the feedback voltage U_{high} from the high voltage DC bus. In addition, the reference current $I_{\text{ref\_Boost}}$ generated by the voltage controller with consideration of the feedback current i_{L1} from the inductor L_1 are used to produce the control variable by the step-up mode current controller. As a result, the corresponding three gate signals $S_1 \sim S_3$ are generated by the PWM generator in the step-up mode.

2). When $I_{\text{sgn}} < 0$, the controller switches the converter to operate in the step-down mode. Similarly, the step-down mode reference voltage $U_{\text{ref-Buck}}$ is given in the step-down mode voltage controller with the feedback voltage U_{low} from the super capacitor bank. In addition, the reference current $I_{\text{ref\_Buck}}$ generated by the voltage controller and the feedback current i_{L1} from the inductor L_1 are also used to produce the control variable by the step-down mode current controller. Therefore, the corresponding three gate signals $S_1 \sim S_3$ are generated by the PWM generator in the step-down mode.

III. PARAMETERS DESIGN AND ANALYSIS

A. Parameters Design of the Power Switches

1. Voltage Stress on the Power Switches

The voltage drop of the power switch is ignored. According to the circuit of the step-up mode, as shown in Fig.3 (a) and (b) (or the circuit of the step-down mode, as shown in Fig.4 (a) and (b)), and the Kirchhoff's voltage law (KVL), the voltage stress on Q_1-Q_3 in the step-up and the step-down modes can be obtained as

$$U_{Q1\_\text{Boost}} = U_{Q2\_\text{Boost}} = U_{Q3\_\text{Boost}} = \frac{U_{\text{low}}}{1 - d_{\text{Boost}}} = \frac{U_{\text{high}}}{1 + d_{\text{Boost}}} \quad (15)$$

$$U_{Q1\_\text{Buck}} = U_{Q2\_\text{Buck}} = U_{Q3\_\text{Buck}} = \frac{U_{\text{low}}}{d_{\text{Buck}}} = \frac{U_{\text{high}}}{2 - d_{\text{Buck}}} \quad (16)$$

where $d_{\text{Boost}} = 1 - d_{\text{Buck}}$. Therefore, the voltage stress on Q_1-Q_3 is the same both in the step-up and step-down modes, according to (15) and (16).

2. Current Stress on the Power Switches

Similarly, according to the circuit of the step-up mode, as shown in Fig.3 (a) and (b) (or the circuit of the step-down mode, as shown in Fig.4 (a) and (b)), and the Kirchhoff's current law (KCL), the current stress on Q_1-Q_3 in the step-up and the step-down modes can be obtained as

$$\begin{cases} I_{Q1\_Boost} = \dfrac{2}{1-d_{Boost}} I_{high} \\ I_{Q2\_Boost} = I_{Q3\_Boost} = -\dfrac{1}{1-d_{Boost}} I_{high} \end{cases} \quad (17)$$

$$\begin{cases} I_{Q1\_Buck} = -\dfrac{2}{2-d_{Buck}} I_{low} \\ I_{Q2\_Buck} = I_{Q3\_Buck} = \dfrac{1}{2-d_{Buck}} I_{low} \end{cases} \quad (18)$$

where $d_{Boost}=1-d_{Buck}$. As a result, the current stress on Q_1 is twice as big as that of Q_2 and Q_3 both in the step-up and the step-down modes, in terms of (17) and (18).

B. Comparisons with Other Converters

Under the premise of the same duty cycle and without considering the power loss, the proposed topology is compared with the traditional two-level bidirectional DC-DC converter, the bidirectional Buck-Boost converter in [31], the traditional three-level bidirectional DC-DC converter in [10], the quadratic DC-DC converter in [32], the classical Z-source converter in [29], the novel Z-source DC-DC converter in [30], the classical quasi-Z-source bidirectional DC-DC converter in [21] and the bidirectional DC-DC converter with a switched-capacitor cell in [27], as shown in TABLE I and TABLE II. The voltage gain against the duty cycle curves of these seven converters in two modes are plotted in Fig.6. According to TABLE I, TABLE II and Fig.6, when the duty cycle of the proposed converter varies between 0.2 and 0.8, the voltage gain in the step-up mode is between 1.5 and 9, and voltage gain in the step-down mode is between 1/9 and 2/3.

Compared with the traditional two-level bidirectional DC-DC converter and Buck-Boost converter in [31], the proposed converter needs an additional power switch, and the current stress on the power switches is relatively large. However, it not only greatly reduces the voltage stress across the power switches, but also expands the voltage gain range. Although the switch voltage and current stresses of the proposed converter

are slightly higher than those of the traditional three-level bidirectional converter in [10], the former requires less number of power switches. Moreover, the voltage gain range is improved more. Compared with the quadratic converter in [32], the proposed one requires an extra capacitor, but reduces one power switch. In addition, the voltage and current stresses on the power switches of the proposed converter are reduced significantly. Although the former has a higher voltage gain, its cascaded structure determines its efficiency is lower than the proposed converter. Compared with the classical Z-source and quasi-Z-source DC-DC converters in [21] and [29], the proposed converter needs the same number of components as those converters. However, the proposed converter remarkably reduces the voltage and current stresses on the power switches, at the cost of reducing the voltage gain a bit, and it has a common ground. Compared with the novel Z-source DC-DC converter in [30], the proposed one requires an extra power switch, but reduces one inductor. In addition, the voltage and current stresses on the power switches of the proposed converter are reduced significantly, and it still has the advantage of a common ground. Compared with the bidirectional DC-DC converter with a switched- capacitor cell in [27], the advantage of the proposed converter lies in an absolute common ground structure, although they have the same number of components, the same reduced voltage and current stresses, and the same voltage gain.

TABLE I COMPARISON ON NUMBER OF COMPONENTS

Topology	Power switch	Capacitor	Inductor
Proposed converter	3	4	2
Two-level converter	2	2	1
Buck-Boost converter in [31]	2	2	1
Three-level converter in [10]	4	3	1
Quadratic converter in [32]	4	3	2
Classical Z-source converter in [29]	3	4	2
Novel Z-source converter in [30]	2	4	3
Classical Quasi-Z-source converter in [21]	3	4	2
Switched-capacitor converter in [27]	3	4	2

TABLE II COMPARISON OF VOLTAGE GAIN AND VOLTAGE AND CURRENT STRESSES

Mode	Topology	Voltage gain	Voltage stress	Current stress		
				Q_1	Q_2	$Q_3(\&Q_4)$
	Proposed converter	$(1+d_{Boost})/(1-d_{Boost})$	$U_{high}/(1+d_{Boost})$	$2I_{high}/(1-d_{Boost})$	$I_{high}/(1-d_{Boost})$	
	Two-level converter	$1/(1-d_{Boost})$	U_{high}	$I_{high}/(1-d_{Boost})$		/
	Buck-Boost converter in [31]	$d_{Boost}/(1-d_{Boost})$	U_{high}/d_{Boost}	$I_{high}d_{Boost}/(1-d_{Boost})$		/
	Three-level converter in [10]	$1/(1-d_{Boost})$	$U_{high}/2$	$I_{high}/(1-d_{Boost})$		
Step-up mode	Quadratic converter in [32]	$1/(1-d_{Boost})^2$	$U_{high}\&(1-d_{Boost})U_{high}$	$I_{high}/(1-d_{Boost})^2$		$I_{high}/(1-d_{Boost})$
	Classical Z-source converter in [29]	$1/(1-2d_{Boost})$	U_{high}	$2I_{high}/(1-2d_{Boost})$		$I_{high}/(1-d_{Boost})$
	Novel Z-source converter in [30]	$(1-d_{Boost})/(1-2d_{Boost})$	$U_{high}/(1-d_{Boost})$	$I_{high}(1-d_{Boost})/(1-2d_{Boost})$		/
	Classical Quasi-Z-source	$1/(1-2d_{Boost})$	U_{high}	$2I_{high}/(1-2d_{Boost})$	$I_{high}/((1-2d_{Boost})(1-d_{Boost}))$	$I_{high}/(1-d_{Boost})$

|					
	converter in [21]				
	Switched-capacitor converter in [27]	$(1+d_{Boost})/(1-d_{Boost})$	$U_{high}/(1+d_{Boost})$	$2I_{high}/(1-d_{Boost})$	$I_{high}/(1-d_{Boost})$
Step-down mode	Proposed converter	$d_{Buck}/(2-d_{Buck})$	$U_{high}/(2-d_{Buck})$	$2I_{low}/(2-d_{Buck})$	$I_{low}/(2-d_{Buck})$
	Two-level converter	d_{Buck}	U_{high}	I_{low}	/
	Buck-Boost converter in [31]	$d_{Buck}/(1-d_{Buck})$	$U_{high}/(1-d_{Buck})$	I_{low}	/
	Three-level converter in [10]	d_{Buck}	$U_{high}/2$	I_{low}	
	Quadratic converter in [32]	d_{Buck}^2	$U_{high}\&d_{Buck}\,U_{high}$	I_{low}	$I_{low}d_{Buck}$
	Classical Z-source converter in [29]	$2d_{Buck}-1$	U_{high}	$2I_{low}$	$(2d_{Buck}-1)I_{low}/\,d_{Buck}$
	Novel Z-source converter in [30]	$(2d_{Buck}-1)/d_{Buck}$	$(2-d_{Buck})U_{high}$	I_{low}	/
	Classical Quasi-Z-source converter in [21]	$2d_{Buck}-1$	U_{high}	$2I_{low}$	I_{low}/d_{Buck} $(2d_{Buck}-1)I_{low}/d_{Buck}$
	Switched-capacitor converter in [27]	$d_{Buck}/(2-d_{Buck})$	$U_{high}/(2-d_{Buck})$	$2I_{low}/(2-d_{Buck})$	$I_{low}/(2-d_{Buck})$
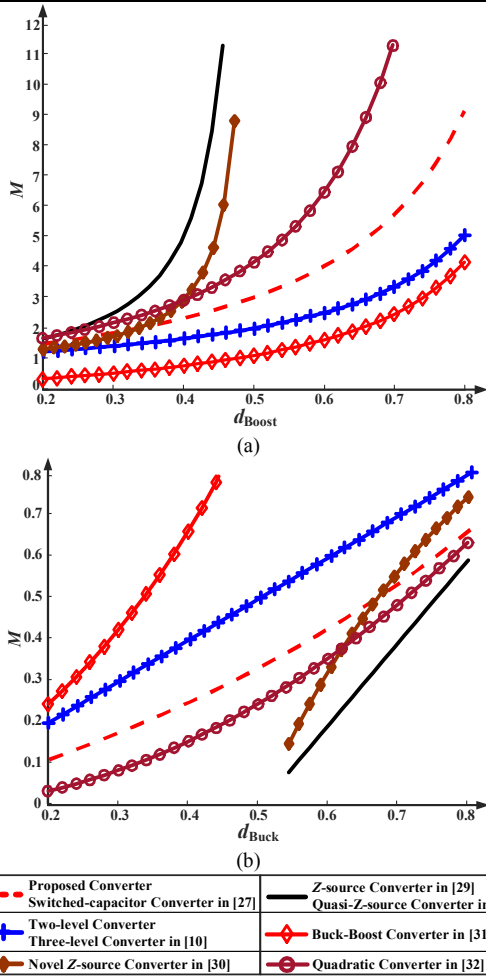
Fig.6 Comparisons of voltage gain against duty cycle. (a) Step-up mode. (b) Step-down mode.

C. Small Signal Analysis and Voltage Loop Controller Design

It is assumed that the inductor currents $i_{L1}(t)$, and $i_{L2}(t)$, capacitor voltages $u_{C1}(t)$, $u_{C2}(t)$, $u_{Clow}(t)$ and $u_{Chigh}(t)$ are the state variables. As shown in Fig.3 (b) and Fig.4 (a), the capacitor voltages $u_{C1}(t)$, $u_{C2}(t)$ and $u_{Chigh}(t)$ are mutually coupled, and there is an invalid state variable. By introducing the series resistance r of the capacitor C_{high}, the coupling between the capacitors C_1, C_2 and C_{high} can be removed to avoid

an invalid state variable.

When the inductor current ripple and the capacitor voltage ripple are neglected, the state space averaging method can be adopted to derive the small signal AC equation of the proposed converter in the step-up mode:

$$
\begin{bmatrix} \dfrac{d\hat{i}_{L1}(t)}{dt} \\ \dfrac{d\hat{i}_{L2}(t)}{dt} \\ \dfrac{d\hat{u}_{C1}(t)}{dt} \\ \dfrac{d\hat{u}_{C2}(t)}{dt} \\ \dfrac{d\hat{u}_{Chigh}(t)}{dt} \end{bmatrix} = \begin{bmatrix} 0 & 0 & -\dfrac{1-D}{L_1} & 0 & 0 \\ 0 & -\dfrac{rD}{L_2} & \dfrac{1}{L_2} & -\dfrac{D}{L_2} & -\dfrac{1-D}{L_2} \\ \dfrac{1-D}{C_1} & -\dfrac{1}{C_1} & -\dfrac{1-D}{C_1 r} & -\dfrac{1-D}{C_1 r} & \dfrac{1-D}{C_1 r} \\ 0 & \dfrac{D}{C_2} & -\dfrac{1-D}{C_2 r} & -\dfrac{1-D}{C_2 r} & \dfrac{1-D}{C_2 r} \\ 0 & \dfrac{1-D}{C_{high}} & \dfrac{1-D}{C_{high} r} & \dfrac{1-D}{C_{high} r} & -\dfrac{1}{C_{high} R}-\dfrac{1-D}{C_{high} r} \end{bmatrix} \begin{bmatrix} \hat{i}_{L1}(t) \\ \hat{i}_{L2}(t) \\ \hat{u}_{C1}(t) \\ \hat{u}_{C2}(t) \\ \hat{u}_{Chigh}(t) \end{bmatrix}
$$

$$
+ \begin{bmatrix} \dfrac{1}{L_1} \\ 0 \\ 0 \\ 0 \\ 0 \end{bmatrix} \hat{u}_{in}(t) + \begin{bmatrix} 0 & 0 & \dfrac{1}{L_1} & 0 & 0 \\ 0 & -\dfrac{r}{L_2} & 0 & -\dfrac{1}{L_2} & \dfrac{1}{L_2} \\ -\dfrac{1}{C_1} & 0 & \dfrac{1}{C_1 r} & \dfrac{1}{C_1 r} & -\dfrac{1}{C_1 r} \\ 0 & \dfrac{1}{C_2} & \dfrac{1}{C_2 r} & \dfrac{1}{C_2 r} & -\dfrac{1}{C_2 r} \\ 0 & -\dfrac{1}{C_{high}} & -\dfrac{1}{C_{high} r} & -\dfrac{1}{C_{high} r} & \dfrac{1}{C_{high} r} \end{bmatrix} \begin{bmatrix} I_{L1} \\ I_{L2} \\ U_{C1} \\ U_{C2} \\ U_{Chigh} \end{bmatrix} \hat{d}(t) \quad (19)
$$

$$
\hat{u}_{high}(t) = \begin{bmatrix} 0 & 0 & 0 & 0 & 1 \end{bmatrix} \begin{bmatrix} \hat{i}_{L1}(t) & \hat{i}_{L2}(t) & \hat{u}_{C1}(t) & \hat{u}_{C2}(t) & \hat{u}_{Chigh}(t) \end{bmatrix}^T
$$

By substituting the corresponding component parameters shown in TABLE III into (19), the control to output voltage transfer function of the proposed converter in the step-up mode can be obtained as follows:

$$
G_{u_{high}d_{Boost}}(s) = \frac{\hat{u}_{high}(s)}{\hat{d}_{Boost}(s)} \quad (20)
$$

$$
= \frac{-2.7\times10^3 \cdot s^4 - 8.8\times10^8 \cdot s^3 + 1.9\times10^{13} \cdot s^2 - 5.2\times10^{15} \cdot s + 7.5\times10^{19}}{s^5 + 1.7\times10^5 \cdot s^4 + 8.8\times10^6 \cdot s^3 + 8.6\times10^{11} \cdot s^2 + 7.3\times10^{12} \cdot s + 7.7\times10^{16}}
$$

Similarly, the small signal AC equation of the converter in the step-down mode can be derived:

$$\begin{bmatrix} \dfrac{d\hat{i}_{L1}(t)}{dt} \\ \dfrac{d\hat{i}_{L2}(t)}{dt} \\ \dfrac{d\hat{u}_{C1}(t)}{dt} \\ \dfrac{d\hat{u}_{C2}(t)}{dt} \\ \dfrac{d\hat{u}_{Clow}(t)}{dt} \end{bmatrix} = \begin{bmatrix} 0 & 0 & \dfrac{D}{L_1} & 0 & -\dfrac{1}{L_1} \\ 0 & -\dfrac{r(1-D)}{L_2} & -\dfrac{1}{L_2} & \dfrac{1-D}{L_2} & 0 \\ -\dfrac{D}{C_1} & \dfrac{1}{C_1} & -\dfrac{D}{C_1 r} & -\dfrac{D}{C_1 r} & 0 \\ 0 & -\dfrac{1-D}{C_2} & \dfrac{D}{C_2 r} & -\dfrac{D}{C_2 r} & 0 \\ \dfrac{1}{C_{low}} & 0 & 0 & 0 & -\dfrac{1}{C_{low}R} \end{bmatrix} \begin{bmatrix} \hat{i}_{L1}(t) \\ \hat{i}_{L2}(t) \\ \hat{u}_{C1}(t) \\ \hat{u}_{C2}(t) \\ \hat{u}_{Clow}(t) \end{bmatrix}$$

$$+ \begin{bmatrix} 0 \\ \dfrac{D}{L_2} \\ \dfrac{D}{C_1 r} \\ \dfrac{D}{C_2 r} \\ 0 \end{bmatrix} \hat{u}_{high}(t) + \begin{bmatrix} 0 & 0 & \dfrac{1}{L_1} & 0 & 0 \\ 0 & \dfrac{r}{L_2} & 0 & -\dfrac{1}{L_2} & 0 \\ -\dfrac{1}{C_1} & 0 & -\dfrac{1}{C_1 r} & -\dfrac{1}{C_1 r} & 0 \\ 0 & \dfrac{1}{C_2} & -\dfrac{1}{C_2 r} & -\dfrac{1}{C_2 r} & 0 \\ 0 & 0 & 0 & 0 & 0 \end{bmatrix} \begin{bmatrix} I_{L1} \\ I_{L2} \\ U_{C1} \\ U_{C2} \\ U_{Clow} \end{bmatrix} \hat{d}(t) + \begin{bmatrix} 0 \\ \dfrac{\hat{d}(t)}{L_2} \\ \dfrac{\hat{d}(t)}{C_1 r} \\ \dfrac{\hat{d}(t)}{C_2 r} \\ 0 \end{bmatrix} U_{high} \quad (21)$$

$$\hat{u}_{low}(t) = \begin{bmatrix} 0 & 0 & 0 & 0 & 1 \end{bmatrix} \begin{bmatrix} \hat{i}_{L1}(t) & \hat{i}_{L2}(t) & \hat{u}_{C1}(t) & \hat{u}_{C2}(t) & \hat{u}_{Clow}(t) \end{bmatrix}^{T}$$

By substituting the corresponding component parameters shown in TABLE III into (21), the control to output voltage transfer function of the proposed converter in the step-down mode can also be obtained as follows:

$$G_{u_{low}d_{Buck}}(s) = \frac{\hat{u}_{low}(s)}{\hat{d}_{Buck}(s)}$$

$$= \frac{1.3 \times 10^{-10} s^3 - 4.0 \times 10^{-6} s^2 + 2.0 s \times 10^{-3} - 43.74}{9.4 \times 10^{-20} s^5 + 2.6 \times 10^{-14} s^4 - 4.0 \times 10^{-9} s^3 - 1.6 \times 10^{-7} s^2 - 4.7 \times 10^{-2} s - 1} \quad (22)$$

The proposed converter adopts an output voltage loop, and the voltage loop control scheme can be obtained as shown in Fig.7, where $G_{uod}(s)$ is the control to output voltage transfer function of the proposed converter, $G_m(s)$ is the transfer function of pulse-width modulator, $H(s)$ is the feedback transfer function and $G_c(s)$ is the voltage controller transfer function. In the closed-loop system of the proposed converter, the transfer functions $G_m(s)=1$, $H(s)=1$ are unitized, and the transfer function $G_c(s)$ of the PI (Proportional-Integral) voltage controller is shown in (23).Therefore, by adjusting the PI parameters K_p and K_i of the voltage loop controller, the closed-loop system of the proposed converter can achieve a better stability performance.
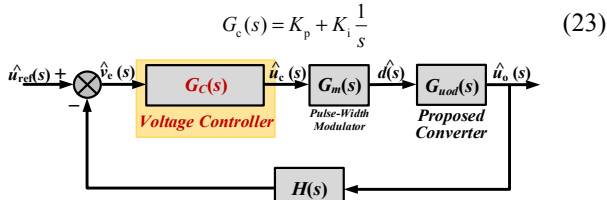
$$G_c(s) = K_p + K_i \frac{1}{s} \quad (23)$$

Fig.7 Voltage loop control scheme of the proposed converter.

As to the output voltage closed-loop system of the proposed converter, when the converter operates in the step-up mode, the PI voltage controller parameters are $K_p=0.001$, and $K_i=0.0001$. Therefore, the corresponding open-loop transfer function $G_{0\_Boost}(s)$ can be obtained as follows:

$$G_{0\_Boost}(s) = G_c(s) G_m(s) G_{u_{high}d_{Boost}}(s) H(s)$$

$$= \frac{-2.7 \cdot s^5 - 8.8 \times 10^5 \cdot s^4 + 1.9 \times 10^{10} \cdot s^3 - 5.2 \times 10^{12} \cdot s^2 + 7.5 \times 10^{16} \cdot s + 7.5 \times 10^{15}}{s^6 + 1.7 \times 10^5 \cdot s^5 + 8.8 \times 10^6 \cdot s^4 + 8.6 \times 10^{11} \cdot s^3 + 7.3 \times 10^{12} \cdot s^2 + 7.7 \times 10^{16} \cdot s}$$

$$(24)$$

Similarly, when the converter operates in the step-down mode, the PI voltage controller parameters are $K_p=0.0015$, and $K_i=0.01$. Thus, the corresponding open-loop transfer function $G_{0\_Buck}(s)$ can be obtained as follows:

$$G_{0\_Buck}(s) = G_c(s) G_m(s) G_{u_{low}d_{Buck}}(s) H(s)$$

$$= \frac{1.1 \times 10^6 \cdot s^4 + 1.2 \times 10^{11} \cdot s^3 + 6.6 \times 10^{12} \cdot s^2 + 6.7 \times 10^{17} \cdot s + 4.5 \times 10^{18}}{s^6 + 1.1 \times 10^5 \cdot s^5 + 5.6 \times 10^7 \cdot s^4 + 1.1 \times 10^{12} \cdot s^3 + 2.5 \times 10^{14} \cdot s^2 + 2.8 \times 10^{18} \cdot s} \quad (25)$$

As a result, the Bode diagrams of the open-loop transfer functions with the PI voltage controllers in the step-up and step-down operating modes can be obtained as shown in Fig.8 (a) and Fig.8 (b), respectively, in terms of (24) and (25). It can be seen that when the proposed converter operates in the step-up and step-down modes, the amplitude margin K_g and the phase margin γ are both greater than 0. Therefore, the closed-loop system of the proposed converter, which adopts the PI voltage controller, can operate stably.
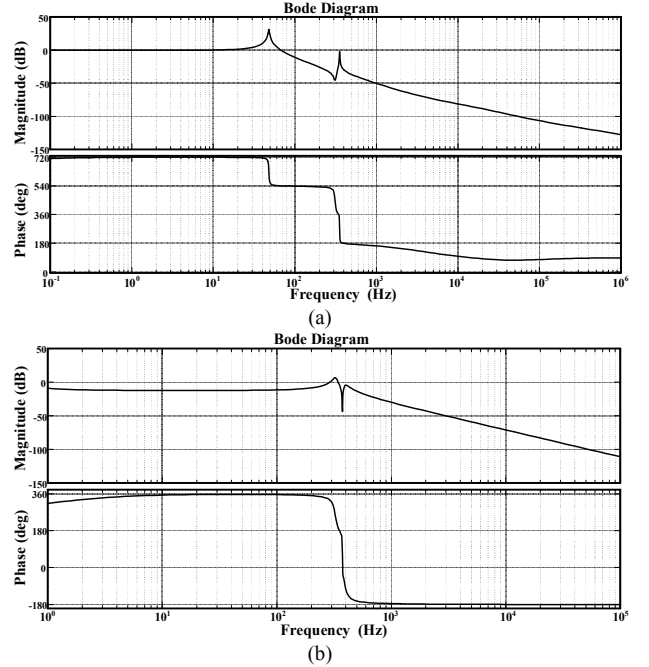
(a)

(b)

Fig.8 Bode plots of the small-signal open-loop transfer functions with PI voltage controllers. (a) The step-up mode. (b) The step-down mode.

IV. EXPERIMENTAL RESULTS AND ANALYSIS

In order to validate the effectiveness of the proposed converter, a 300W prototype is developed, as shown in Fig.9. The specific parameters of the experimental prototype are given in TABLE III. A Texas Instruments microcontroller TMS32028335 is used for the voltage loop controller.
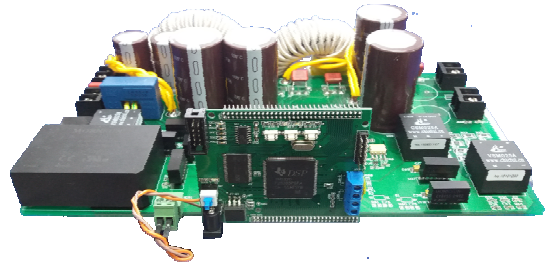
Fig.9 Prototype of the proposed converter.

TABLE III EXPERIMENTAL PARAMETERS OF THE CONVERTER

Parameter	Values
Rated power: P_n	300W
Filtering capacitors: C_{low}/C_{high}	470μF
Switched capacitors: C_1/C_2	520μF
Inductor 1: L_1	434μH
Inductor 2: L_2	600μH
High-side voltage: U_{high}	240V
Low-side voltage: U_{low}	40~120V
Switching frequency: f_s	20kHz
Power MOSFETs: Q_1~Q_3	IXTH88N30P

A. Experimental Results in the Step-Up Mode

When the proposed converter operates in the step-up mode at the rated condition, the gate signal and the voltage stress waveforms of Q_1, and the voltage stress waveforms of the synchronous rectifiers Q_2 and Q_3 are shown in Fig.10 and Fig.11, respectively. It can be seen that the voltage stress on Q_1-Q_3 is 140V (slightly higher than half of the high-side voltage), which is consistent with the theoretical calculation.
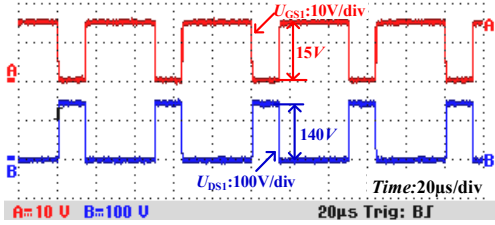
Fig.10 Voltage stress across power switch Q_1 in the step-up mode.
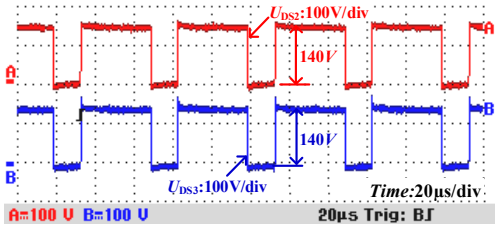
Fig.11 Voltage stress across synchronous rectifiers Q_2-Q_3 in the step-up mode.

At the same condition, the current waveforms of L_1 and L_2 are shown in Fig.12. It can be seen that the current ripple rate of L_1 is about 28.57%, and that of L_2 is about 200% due to its smaller average current value, which satisfy the design requirements of the inductors.
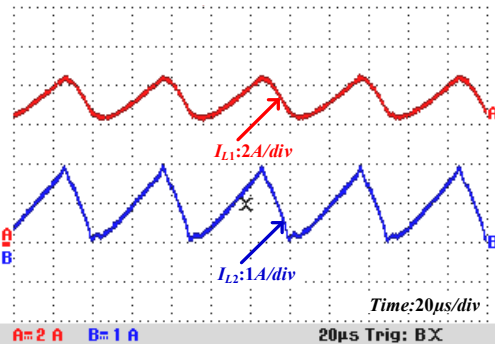

Fig.12 Inductor currents, when U_{low} = 40V, and U_{high} = 240V.

Fig.13 shows the dynamic behavior of the output voltage U_{high} which keeps at 240V, when the input voltage U_{low} changes from 120V to 40V over 11 seconds simulating the continuous discharging of the energy source and its terminal voltage drops.

It illustrates that the converter can achieve a wide voltage gain range from 2 to 6.
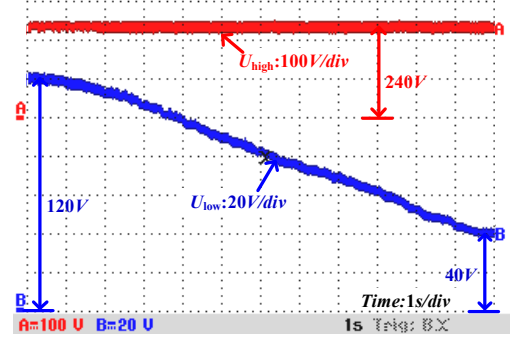
Fig.13 Input voltage U_{low} and output voltage U_{high} when input voltage changes from 120V to 40V.

The output voltage and the load current are shown in Fig.14, when the output power P_o is step changed between 150W and 300W. It can be seen that when the proposed converter operates under the voltage loop controller in the step-up mode, the output voltage U_{high} can be nearly kept at 240V and the transient voltage fluctuation is small enough to be neglected.
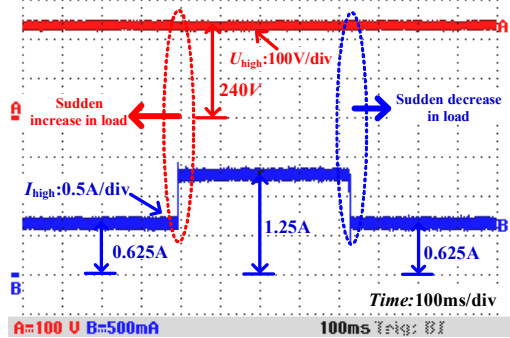
Fig.14 Output voltage and load current when output power P_o is step changed between 300W and 150W in step-up mode.

B. Experimental Results in the Step-Down Mode

When the proposed converter operates in the step-down mode at the rated condition, the gate signal and the voltage stress across Q_2, and the voltage stress across Q_3 and the synchronous rectifier Q_1 are shown in Fig.15 and Fig.16, respectively. It is clear that the voltage stress on Q_1-Q_3 is still 140V (slightly higher than half of the high-side voltage), which also agrees with the theoretical calculation.
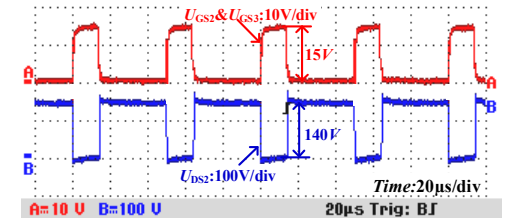
Fig.15 Voltage stress across Q_2.
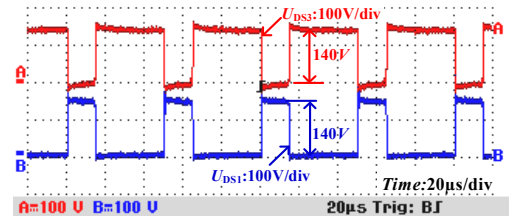
Fig.16 Voltage stress across Q_3 and synchronous rectifier Q_1.

At the same condition, the currents of L_1 and L_2 are shown in Fig.17. It can be seen that the current ripple rate of L_1 is about 26.67% and that of L_2 is about 200% due to its smaller average current value, which also satisfy the design requirements of the inductors.

Fig.18 shows the dynamic behavior of the output voltage U_{low} when the input voltage U_{high} maintains at 240V, and the output voltage U_{low} is controlled to change from 40V to 120V. This experimental result is used to simulate the continuous charging of the energy source, and its terminal voltage rises. When the input voltage U_{high} keeps at 240V, the output voltage U_{low} increases from 40V to 120V within 11 seconds, namely, the converter can obtain a wide voltage gain range from 0.16 to 0.5 in the step-down mode.
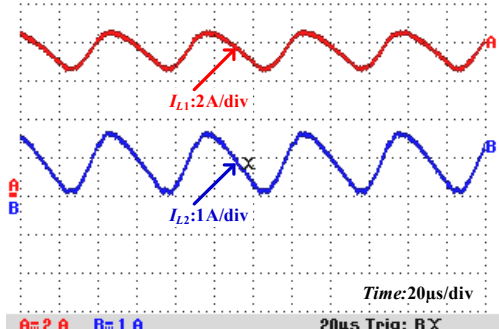

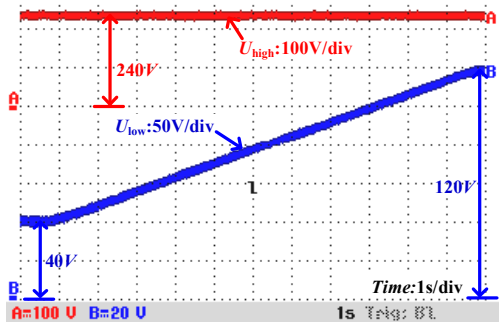Fig.17 Inductors current waveforms, when U_{high} = 240V, U_{low} = 40V.

Fig.18 Input voltage U_{high} and output voltage U_{low} when output voltage changes from 40V to 120V.

The output voltage and the load current are shown in Fig.19, when the output power P_o is step changed between 160W and 320W in the step-down mode. It can be seen that when the proposed converter operates under the output voltage closed loop control in the step-down mode, the output voltage U_{low} can nearly be kept at 40V and the voltage fluctuation is small enough to be neglected.
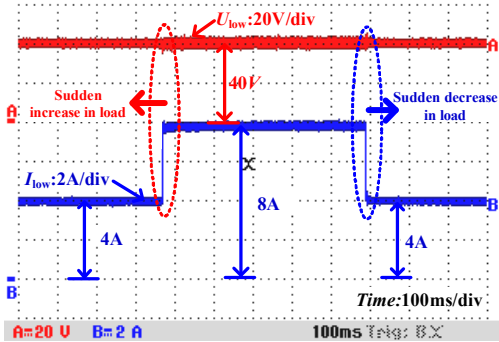

Fig.19 Output voltage and load current when output power P_o is step changed between 320W and 160W in step-down mode.

C. Experimental Results of Bidirectional Power Control of the Proposed Converter

Fig.20 shows the hybrid energy sources system for an electric vehicle, which is comprised of the super capacitor and the battery pack. The super capacitor bank is composed of four CSDWELL's super capacitor modules in series, and the battery pack is comprised of the lithium iron phosphate battery with a capacity of 20Ah. In the hybrid energy sources system, the proposed switch-quasi-Z-source bidirectional DC-DC converter is interfaced between the high voltage DC bus and the low voltage super capacitor bank. The battery pack provides the average power for the DC bus through the bidirectional DC-DC converter, boosting the low voltage of the battery pack to match the high voltage of the DC bus.

When the vehicle is accelerating, the super capacitor bank supplies the instantaneous power required from the DC bus by the proposed DC-DC converter rapidly, due to the quick dynamic response characteristics of the super capacitor bank. During this process, the bidirectional DC-DC converter steps up the variable battery pack voltage to keep the constant high voltage of the DC bus with a voltage loop, and provides the average power for the DC bus. When the vehicle decelerates or brakes, the regenerative energy can be absorbed controllably by the super capacitor and the battery packs through the bidirectional DC-DC converters. When the vehicle operates at uniform speed, the battery pack provides the steady energy for the DC bus through the bidirectional DC-DC converter with the corresponding voltage-gain, and charges the super capacitor bank by the proposed converter if it is needed. According to the operating conditions previously described, the hybrid energy sources management system in electric vehicles provides the control signal I_{sgn} for the controller of the proposed converter. Then, the proposed converter can be controlled in the bidirectional power flow modes, according to the control strategy as shown in Fig.5.

The experimental results of the proposed converter in the bidirectional power control modes are shown in Fig.21. The currents I_{sc} and I_{bat} represent the super capacitor current and battery current respectively. It is assumed that the current from the positive polar of the super capacitor bank/battery pack is in the positive polar direction.
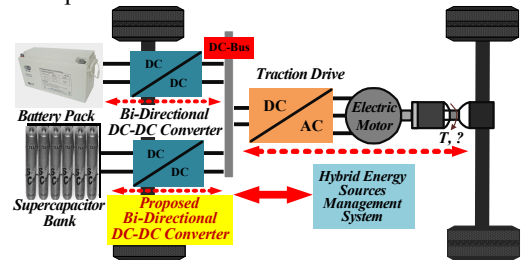

Fig.20 Hybrid energy sources system for an EV.

It can be seen that when the demand DC bus power is changed quickly from 400W to 650W, which simulates the electric vehicle's accelerating process, the control signal I_{sgn} that output from the hybrid energy sources management system is greater than 0. At the same time, the proposed converter responds quickly and operates in the step-up mode. The current I_{sc} increases quickly from 0A to 5A during approximately 20ms, and the super capacitor provides the instantaneous current I_{sc} for

the DC bus, while the output current I_{bat} of the battery increases very slowly. When I_{sc} falls to 0A from 5A, I_{bat} rises gently from 8.8A to 13A, and the battery provides the static power for the DC bus. Similarly, when the demand DC bus power is reduced quickly from 650W to 400W, which simulates the electric vehicle's decelerating process, the control signal I_{sgn} is less than 0. At the same time, the proposed converter responds quickly and operates in the step-down mode. The current I_{sc} increases from zero to -4A over approximately 20ms, and the super capacitor absorbs the instantaneous power from the DC bus. When the current I_{sc} falls to 0A from -5A, the current I_{bat} is gradually reduced from 13A to 8.8A, and the battery absorbs the power from the DC bus very slowly.
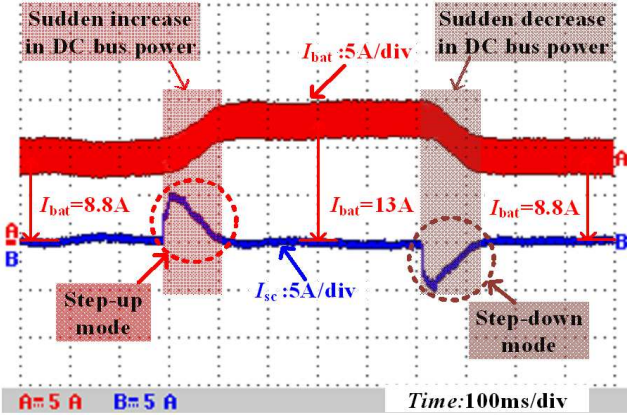

Fig.21 Experimental results of the proposed converter in the bidirectional power control modes.

Therefore, when electric vehicles have a sudden increase or decrease during the accelerating or decelerating process, the proposed converter can respond quickly according to the control signal I_{sgn}. The super capacitor can provide or absorb the instantaneous power to ensure that the current of the battery changes more gently. As a result, the battery can be protected and the dynamic response of the whole powertrain system is improved.

D. Efficiency Analysis of the Proposed Converter

The experimental efficiencies at different voltage gains are shown in Fig.22. The experimental efficiency is measured by the power analyzer YOKOGAWA/WT3000.
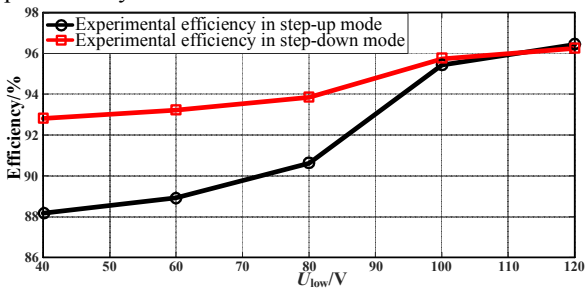

Fig.22 Efficiency of the proposed converter in the step-up and step-down modes with U_{high}=240V, U_{low}=40~120V and P_o=300W.

From Fig.22, the maximum and minimum efficiencies of the proposed converter in the step-up mode are 96.44% and 88.17%, respectively. And the maximum and minimum efficiencies of the proposed converter in the step-down mode are 96.24% and 92.31%, respectively. It is noticed that the maximum measured efficiencies of the proposed converter in the step-up and

step-down modes are very close to those of converters in [10], [16], [17] [25], [27] and [28]. As shown in Fig.22, with the increase of the low-side voltage, the efficiency of the proposed converter increases gradually for the same output power, due to the reduced losses caused by the decreasing input current.

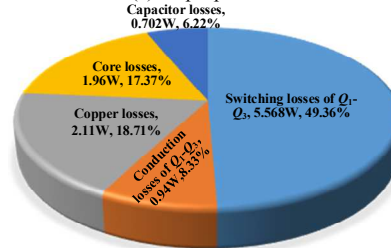### E. Power Loss Analysis of the Proposed Converter

The calculated power loss distributions for the experiment when U_{low}=120V, U_{high}=240V, P_o=300W and d_{Boost}=1-d_{Buck}=0.33 are shown in Fig.23.

When the proposed converter operates in step-up mode, the total losses of the converter are 10.68W, and the loss distribution is shown in Fig.23 (a). By analyzing the power losses distribution, it can be concluded that the major losses come from the switching losses of the power switches Q_1-Q_3 (i.e. P_{2_Boost}=4.98W), which account for 46.63% of the total losses. The conduction losses of all power switches Q_1-Q_3 (i.e. P_{Q_Boost}=0.925W) account for 8.66% of the total losses. In addition to the power losses of the semiconductors, the copper losses P_{Cu_Boost} of inductors L_1 and L_2 is 1.98W, which account for 19.75% of the total losses. And the core losses P_{Fe_Boost} of inductors L_1 and L_2 account for 18.35% of the total losses, which is close to that of the copper losses. The capacitor losses P_{C_Boost} of C_1-C_2 and C_{high} is 0.7W, which account for 6.55% of the total losses.

Similarly, when the proposed converter operates in step-down mode, the total losses of the converter are 11.28W, and the loss distribution is shown in Fig.23 (b). By analyzing the power losses distribution, it can be concluded that the major losses also come from the switching losses of the power switches Q_1-Q_3 (i.e. P_{2_Buck}=5.568W), which account for 49.36% of the total losses. The conduction losses of all power switches Q_1-Q_3 (i.e. P_{Q_Buck}=0.94W) account for 8.33% of the total losses. In addition to the power losses of the semiconductors, the copper losses P_{Cu_Buck} of inductors L_1 and L_2 is 2.11W, which account for 18.71% of the total losses. And the core losses P_{Fe_Buck} of inductors L_1 and L_2 account for 17.37% of the total losses, which is close to that of the copper losses. The capacitor losses P_{C_Buck} of C_1-C_2 and C_{high} is 0.702W, which account for 6.22% of the total losses.
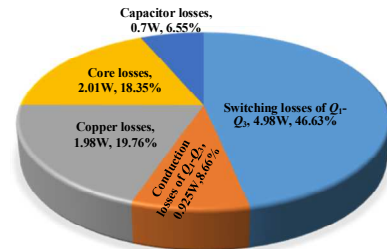
(a) Step-up mode.

(b) Step-down mode.

Fig.23 Calculated power loss distributions for the experiment when U_{low}=120V, U_{high}=240V, P_o=300W and d_{Boost}=1-d_{Buck}=0.33.

V. CONCLUSION

A non-isolated switched-quasi-Z-source DC-DC converter for electric vehicles with the hybrid energy sources has been proposed in this paper, which is based on the traditional quasi-Z-source bidirectional DC-DC converter. The proposed converter benefits from a wide voltage gain range in step-up and step-down modes and an absolute common ground. In addition, the bidirectional converter has a simple structure with three active power switches, and their voltage stress is lower. The proposed converter also has good dynamic and static performance. Therefore, it can be applied as the power interface between the low voltage battery pack/super capacitor bank and the high voltage DC bus in the hybrid energy sources system for EVs.

REFERENCES

[1] K. W. Hu, and C. M. Liaw, "Incorporated Operation Control of DC Microgrid and Electric Vehicle," *IEEE Trans. Ind. Electron.*, vol.63, no. 1, pp. 202-215, Jan. 2016.

[2] M. Yilmaz and P. Krein, "Review of benefits and challenges of vehicleto-grid technology," in *Proc. IEEE Energy Convers. Congr. Expo.*, Raleigh, NC, USA, Sep. 2012, pp. 3082–3089.

[3] M. Kesler, M. C. Kisacikoglu, and L. M. Tolbert, "Vehicle-to-grid reactive power operation using plug-in electric vehicle bidirectional offboard charger," *IEEE Trans. Ind. Electron.*, vol. 61, no. 12, pp. 6778–6784, Dec. 2014.

[4] Y. Xue, L. Chang, S. B. Kjaer, J. Bordonau, and T. Shimizu, "Topologies of single-phase inverters for small distributed power generators: An overview," *IEEE Trans. Power Electron.*, vol. 19, no. 5, pp. 1305–1314, Sep. 2004.

[5] M. N. Marwali and A. Keyhani, "Control of distributed generation systems—Part I: voltages and current control," *IEEE Trans. Power Electron.*, vol. 19, no. 6, pp. 1541–1550, Nov. 2004.

[6] M. Yilmaz and P. T. Krein, "Review of battery charger topologies, charging power levels, and infrastructure for plug-in electric and hybrid vehicles," *IEEE Trans. Power. Electron.*, vol. 28, no. 5, pp. 2151–2169, May. 2013.

[7] C. Liu, K. T. Chau, D. Wu, and S. Gao, "Opportunities and challenges of vehicle-to-home, vehicle-to-vehicle, and vehicle-to-grid technologies," *Proc. IEEE*, vol. 101, no. 11, pp. 2409–2427, Nov. 2013.

[8] M. Choi, S. Kim, and S. Seo, "Energy management optimization in a battery/supercapacitor hybrid energy storage system," *IEEE Trans. Smart Grid*, vol. 3, no. 1, pp. 463–472, Mar. 2012.

[9] Y. Zhang, Z. Jiang, and X. Yu, "Control strategies for battery/supercapacitor hybrid energy storage systems," in *Proc. IEEE Energy 2030 Conf.*, Nov. 2008, pp. 1–6

[10] K. Jin, M. Yang, X. Ruan, and M. Xu, "Three-level bidirectional converter for fuel-cell/battery hybrid power system," *IEEE Trans. Ind. Electron.*, vol. 57, no. 6, pp. 1976–1986, Jun. 2010.

[11] P. J. Grbovic, P. Delarue, P. Le Moigne, and P. Bartholomeus, "A bi-directional three-level dc-dc converter for the ultra-capacitor applications," *IEEE Trans. Ind. Electron.*, vol. 57, no. 10, pp. 3415–3430, Oct. 2010.

[12] S. Busquets-Monge, S. Alepuz, and J. Bordonau, "A novel bidirectional multilevel boost-buck dc-dc converter," *IEEE Trans. Power Electron.*, vol. 26, no. 8, pp. 2172–2183, Aug. 2011.

[13] I.-D. Kim, S.-H. Paeng, J.-W. Ahn, E.-C. Nho, and J.-S. Ko, "New bidirectional ZVS PWM Sepic/Zeta DC–DC converter," in *Proc. IEEE ISIE Conf. Rec.*, 2007, pp. 555–560.

[14] C. Li, L. Herrera, J. Jia, L. Fu, A. Isurin, A. Cook, Y. Huang and J. Wang, "Design and implementation of a bidirectional isolated Cuk converter for low-voltage and high-current automotive DC source applications," *IEEE Trans. Veh. Technol.*, vol. 63, no. 6, pp. 2567–2577, Jul. 2014.

[15] H.-Y. Lee, T.-J. Liang, J.-F. Chen, and K.-H. Chen, "Design and implementation of a bidirectional SEPIC-Zeta DC-DC Converter," in *Proc.*

[16] Y.-P. Hsieh, J.-F. Chen, L.-S. Yang, C.-Y. Wu, and W.-S. Liu, "High conversion-ratio bidirectional DC-DC converter with coupled inductor," *IEEE Trans. Ind. Electron.*, vol. 61, no. 1, pp. 210-222, Jan. 2014.

[17] L. Jiang, X. Zhang, C. Yin, C. Mi, S. Li, and M. Zhang, "A novel soft-switching bidirectional dc–dc converter with coupled inductors," *IEEE Trans. Ind. Appl.*, vol. 49, no. 6, pp. 2730–2740, Nov./Dec. 2013.

[18] H Wu, K Sun, L Chen, and L Zhu, "High step-up/step-down soft-switching bidirectional DC–DC converter with coupled-inductor and voltage matching control for energy storage systems," *IEEE Trans. Ind. Electron.*, vol. 63, no. 5, pp. 2892-2903, May. 2016.

[19] H Shen, B Zhang, D Qiu, and L Zhou, "A common grounded Z-source DC–DC converter with high voltage gain," *IEEE Trans. Ind. Electron.*, vol. 63, no. 5, pp. 2925-2935, Jan. 2016.

[20] G. Zhang, Z. Li, B. Zhang, D. Qiu, W. Xiao, and W. A. Halang, "A Z-source half-bridge converter," *IEEE Trans. Ind. Electron.*, vol. 61, no. 3, pp. 1269–1279, Mar. 2014.

[21] T. Takiguchi and H. Koizumi, "Quasi-Z-source dc-dc converter with voltage-lift technique," in *Proc. IEEE 39th Annu. Conf. Ind. Electron. Soc.*, Nov. 10–13, 2013, pp. 1191–1196.

[22] Y. Tang, T. Wang, and Y. He, "A switched-capacitor-based active-network converter with high voltage gain," *IEEE Trans. Power Electron.*, vol. 29, no. 6, pp. 2959–2968, Jun. 2014.

[23] Y. Tang, D. Fu, T. Wang, and Z. Xu, "Hybrid switched-inductor converters for high step-up conversion," *IEEE Trans. Ind. Electron.*, vol. 62, no. 3, pp. 1480–1490, Mar. 2015.

[24] Y. Tang, T. Wang, and D. Fu, "Multicell switched-inductor/switched -capacitor combined active-network converters," *IEEE Trans. Power Electron.*, vol. 30, no. 4, pp. 2063–2072, Apr. 2015.

[25] H Ardi, A Ajami, F Kardan, SN Avilagh, "Analysis and implementation of a no-isolated bidirectional DC–DC converter with high voltage gain," *IEEE Trans. Power Electron.*, vol. 63, no. 8, pp.4878–4888, Aug. 2016.

[26] Y. S. Lee and Y. P. Ko, "Switched-capacitor bi-directional converter performance comparison with and without quasi-resonant zero-current switching," *IET Power Electron.*, vol. 3, no. 2, pp. 269–278, Mar. 2010.

[27] O. Cornea, GD. Andreescu, N. Muntean, and D. Hulea, "Bidirectional power flow control in a DC microgrid through a switched-capacitor cell hybrid DC–DC converter," *IEEE Trans. Ind. Electron.*, vol. 64, no. 4, pp. 3012–3022, Apr. 2017.

[28] L. S. Yang and T. J. Liang, "Analysis and implementation of a novel bidirectional dc–dc converter," *IEEE Trans. Ind. Electron.*, vol. 59, no. 1, pp. 422–434, Jan. 2012.

[29] X. Fang and X. Ji, "Bidirectional power flow Z-source dc-dc converter," in *Proc. IEEE Veh. Power Propulsion Conf. (VPPC'08)*, pp.1–5.

[30] X. Fang, "A novel Z-source dc-dc converter," in *Proc. IEEE ICIT*, 2008, pp. 1–4.

[31] S. Busquets-Monge, S. Alepuz, and J. Bordonau, "A bidirectional multilevel boost-buck dc-dc converter," *IEEE Trans. Power Electron.*, vol. 26, no. 8, pp. 2172–2183, Aug. 2011.

[32] A. Ahmad, RK. Singh, R. Mahanty, "Bidirectional quadratic converter for wide voltage conversion ratio," in *Proc. IEEE Int. Conf. PEDES*, 2016, pp. 1-5.

Yun Zhang (M'13) was born in Jiangsu, China, in 1980. He received the B.S. and M.S. degrees in electrical engineering from the Harbin University of Science and Technology, Harbin, China, in 2003 and 2006, respectively, and the Ph.D. degree in electrical engineering from the Harbin Institute of Technology, Harbin, China, in 2010.

In 2010, he joined the Tianjin University, Tianjin, China, as a Lecturer in the School of Electrical and Information Engineering, where he is currently an Associate Professor. His current research interests include topologies, modulation, and control strategies of power converters for electric vehicles and microgrids.

Dr. Zhang is an Associate Editor of the Journal of Power Electronics.

Qiangqiang Liu was born in Jiangsu, China. He received his B.S. degree in Electrical Engineering from the China University of Mining and Technology, Xuzhou, Jiangsu, China, in 2016. He started pursing his M.S. degree in Electrical Engineering from the Tianjin University, Tianjin, China, in 2016.

His current research interests include topologies, modulation, and control strategies of DC-DC converters.

Jing Li (M'15) received the B.Eng. (Hons.) and M.Sc. (Distinction) degrees both in control science and engineering from the Beijing Institute of Technology, Beijing, China, in 1999, and 2002, respectively, and the Ph.D. degree in electrical engineering from the University of Nottingham, Nottingham, U.K., in 2010.

She was a Research Fellow with the Power Electronic, Machine and Control Group, University of Nottingham. She is currently a Lecturer at the Department of Electrical and Electronic Engineering, University of Nottingham Ningbo China, Ningbo, China. Her research interests include condition monitoring for motor drive systems and power distribution systems and advanced control and design of motor drive systems.

Mark Sumner (SM'05) received the B.Eng. degree in electrical and electronic engineering from Leeds University, Leeds, U.K., in 1986, and the Ph.D. degree in induction motor drives from the University of Nottingham, Nottingham, U.K., in 1992.

He was with Rolls Royce, Ltd., Ansty, U.K. He was a Research Assistant with the University of Nottingham, where he became a Lecturer in October 1992, and is currently a Professor of electrical energy systems. His research interests include control of power electronic systems including sensorlessmotor drives, diagnostics and prognostics for drive systems, power electronics for enhanced power quality, and novel power system fault location strategies.